The Total n-p Scattering Cross Section at 4.75 Mev*

E. M. Hafner, W. F. Hornyak, C. E. Falk, G. Snow, and T. Coor
Brookhaven National Laboratory, Upton, New York

(Received September 9, 1952)

Attenuation measurements in good geometry on polyethylene and graphite scatterers with transmissions from 0.30 to 0.65 have been made. A thin-walled gas target was used, producing forward d-d neutrons at a mean energy of 4.749±0.009 Mev. Care was taken to minimize uncertainties arising from neutrons of other energies, from unshadowed background, and from impurities in the samples. The geometry was such that multiple scattering-in contributed no more than 0.12 percent to the total uncertainty. Checks against rate-dependent sensitivity of the detector revealed no effects greater than 0.15 percent. The total n-p scattering cross section deduced from the measurements is $1.690\pm0.006_6$ barns, where the probable error has been increased from the statistical error of 0.002_4 barn to include the energy uncertainty and estimates of possible systematic effects. Values of $r_{0s}^{(n-p)}$, the singlet effective range of the n-p interaction, obtained from this result for several potential shapes, are compared with corresponding values of $r_{0s}^{(p-p)}$. The validity of the hypothesis of charge independence is found to depend on the potential shape assumed.

I. INTRODUCTION

A STUDY of the scattering of neutrons by protons and a comparison with the scattering of protons by protons can yield fundamental information about the nature of nuclear forces. The effective range theory[1,2] of nuclear scattering shows that the neutron-proton scattering cross section is approximately determined up to 10 Mev by four parameters: the triplet and singlet scattering amplitudes, a_t and a_s, and the triplet and singlet effective ranges, r_{0t} and r_{0s}. The first three of these parameters have been determined with good precision from measurements of the deuteron binding energy and of neutron-proton scattering cross sections at thermal energies. Measurements of the neutron-proton scattering cross sections at higher energies serve as the most promising method of determining the fourth parameter, r_{0s}. A comparison of the n-p singlet effective range with the measured value of the p-p singlet effective range then serves as a most critical test of the hypothesis of charge independence of nuclear forces.

Salpeter[3] has pointed out that the three parameters a_t, a_s, r_{0t} are known with sufficient accuracy so that a measurement of the total n-p cross section at energies greater than ~2 Mev can yield information about the shape of the neutron-proton interaction potential in addition to the value of r_{0s}. Since the singlet n-p cross section contributes only one quarter of the total cross section, a very precise scattering experiment is needed to obtain the value of r_{0s}. An interpretation[3] of the most recent medium energy cross-section measurements[4] assigns the value $2.6\pm0.5\times10^{-13}$ cm to the effective singlet range in the shape independent approximation, and concludes that the experimental results are not sufficiently accurate to yield information about the shape of the nuclear potential. This result implies charge independence of effective range to an accuracy of 25 percent.

The present experiment is an attempt to provide a more accurate cross section in the medium energy region, that is, at an energy high enough to bring in a significant dependence of cross section on range and low enough to avoid complications introduced by the contributions of angular momenta greater than zero and of relativistic effects. The importance of the shape dependent terms increases in direct proportion to the energy. At the beginning of this work we had been informed[5] that an accurate measurement at 1.3 Mev was in progress. We decided to work at a somewhat higher energy, 5 Mev, principally to obtain a separate evaluation of the singlet effective range, and also in the hope of combining the results to obtain a more definite clue to the potential shape than has hitherto been given.

The measurements were made in the forward beam of neutrons from the $H^2(d,n)He^3$ reaction. Three scatterer diameters were used, the smallest requiring a scattering-in correction of 0.6 percent. The thin-walled target contained deuterium gas in which the energy loss was 195 kev, separated from the accelerator vacuum system by a nickel foil in which the energy loss was 161 kev. Recoil scintillation neutron counters of approximately one percent efficiency were used as detector and monitor. Each counter amplifier fed two independent discriminators and scalers, operating at different counting rates, as a check against scaler pile-up, dead-time effects, and drift of bias. Transmission runs at alternately high and low neutron flux were taken as an additional check against any possible rate dependence. Scatterers were made of polyethylene and graphite, with transmissions between 0.30 and 0.65. The mean effective neutron energy of 4.75 Mev was chosen primarily on the basis that it permitted accurate foil and gas-thickness calibrations to be made, using sharp proton resonances at approximately half the deuteron energy.

The effect of axial neutrons not originating in the target gas was measured by transmission runs under

* Research carried out under contract with the AEC.

[1] H. A. Bethe, Phys. Rev. **76**, 38 (1949).
[2] J. M. Blatt and J. D. Jackson, Phys. Rev. **76**, 18 (1949).
[3] E. E. Salpeter, Phys. Rev. **82**, 60 (1951).
[4] Lampi, Freier, and Williams, Phys. Rev. **80**, 853 (1950).
[5] D. H. Frisch (private communication).

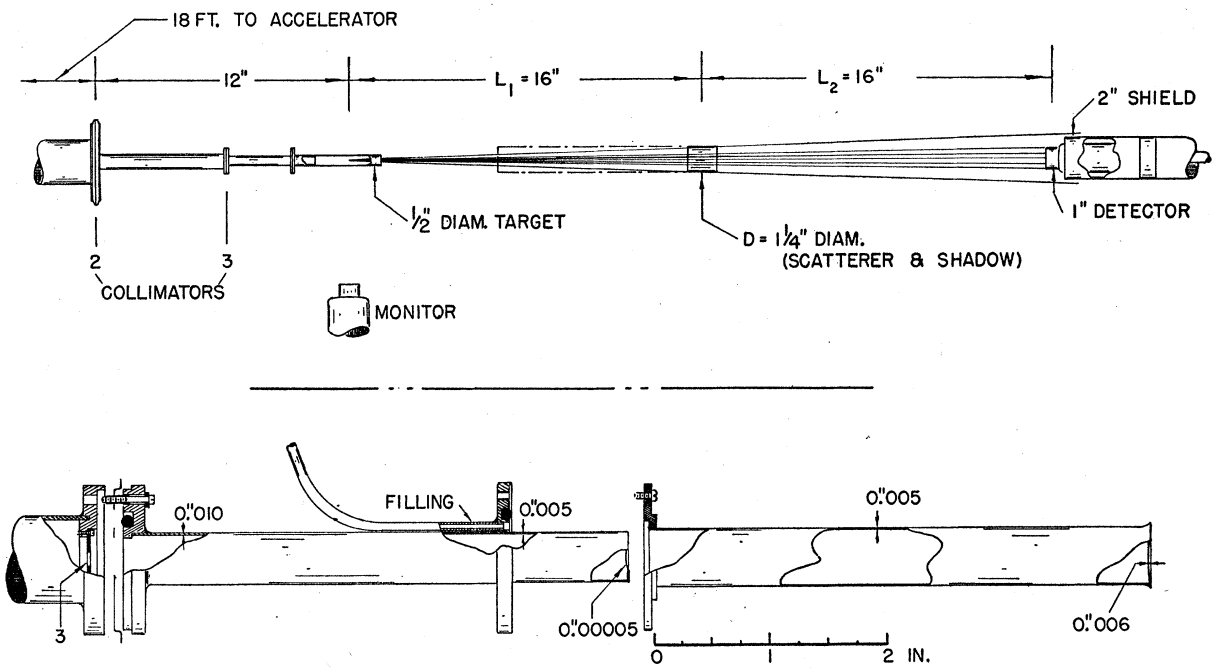

FIG. 1. Geometry of the experiment and exploded view of target assembly. The beam collimators, 2 and 3, are preceded by another aperture 48 in. away, backed by a solid cylinder to scatter out neutrons produced in the slit surface. The minimum scatterer and shadow diameter is shown; the margin of safe shadowing around the detector shield is ¼ in. The detector is fitted with an axial viewing tube for line-up. Target is made of brass, with entrance window of Ni and end-foil of Au. There is also a liner of 0.002-inch Au.

hydrogen filling, and the correction was, on the average, about 0.5 percent of the cross section. The shadow background of 1.5 percent was measured with nickel cylinders of computed transmission 0.0003. Upper limits to scattering-in effects of order higher than the first were estimated and found to be small. An analysis of a total of 209 runs, each with a statistical probable error of about 0.6 percent, at the various diameters and transmissions, checked this estimate and yielded the cross sections quoted in Sec. V.

The design of the experiment involved a number of considerations which are, it is felt, essential to the success of any precise transmission measurement. In the belief that many of these factors have been treated here with greater care than in previous determinations, a fairly detailed discussion of the method is carried out in Sec. II following the order of the summary just given.

II. EXPERIMENTAL METHOD

A. Geometry

The proper choice of geometry in this experiment represents a compromise between two sets of conflicting factors:

(1) In order to obtain a small scattering-in effect, D/L should be small, where D is the scatterer diameter and $L=L_1+L_2$ is the distance from source to detector (see Fig. 1).

(2) From the standpoints of background and intensity, L should be small. If a quantity β be defined as the fraction of unattenuated detectable flux that is not shadowed, it has been observed that β increases roughly as L^2. It is also clear that, if the ion current is fixed and the primary neutron flux at the detector is to be held at a reasonable value, the target thickness and hence the uncertainty in mean neutron energy must increase approximately as L^2.

As a result of first-order scattering-in effects apparent cross sections are lowered by an amount

$$\frac{\Delta\sigma}{\sigma}=\frac{f}{16}\left(\frac{DL}{L_1L_2}\right)^2, \tag{1}$$

where L_1 and L_2 are the distances shown in Fig. 1, and

$$f=\frac{4\pi}{\sigma}\left(\frac{d\sigma}{d\omega}\right)_0 \tag{2}$$

is a measure of the predominance of forward scattering. In the case of scattering by hydrogen, isotropic in the center-of-mass coordinates, a simple calculation shows that in the laboratory frame $f_h=4$. The function $\Delta\sigma/\sigma$ has a minimum at $L_1=L_2=L/2$. The over-all detector diameter, with adequate margin of safety, that must be shadowed is $2\frac{1}{2}$ inches (Sec. IIC). Therefore, the smallest scatterer diameter that can be used under the above optimum selection of L_1 and L_2 is $1\frac{1}{4}$ inch. Our estimate of the probable error of the scattering-in correction (Sec. IV) is one-fifth of the full value of the effect at best geometry. From these considerations it

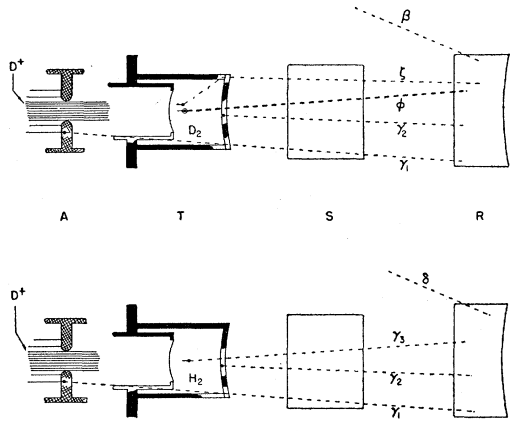

FIG. 2. Schematic view of neutron components with deuterium filling (upper) and hydrogen filling (lower). φ is the primary flux. γ_1 is the forward flux from the surfaces of apertures (A); γ_2 from the Au end-wall of target (T); γ_3 from traces of D_2 with the H_2 filling. ζ is due to wall scattering of primary neutrons. β is the off-axis flux detected by the recoil unit (R) but not shadowed by the scatterer (S), that occurs with D_2 filling; δ is the corresponding flux with H_2 filling. In this experiment, under the geometry of Fig. 1, the components had the following approximate magnitudes relative to φ: $\gamma_1+\gamma_2\simeq 0.02$; $\gamma_3\simeq 0.01$; $\zeta\simeq 0.003$; $\beta\cong 0.015$; $\delta=0.0025$.

follows that an error less than 0.0015 results from a detector distance greater than 25 inches.

It has been found under the prevailing background conditions at this laboratory that $\beta\simeq 1.2\times 10^{-5}L^2$, where L is in inches. The effect of β (Sec. IIG) is to lower apparent cross sections by an amount

$$\frac{\Delta\sigma}{\sigma}=\frac{(1-T)}{T\ln(1/T)}\beta. \tag{3}$$

The estimated uncertainty in this correction assigns a probable error which is one-tenth of its full value. It follows that the detector distance can be increased to 30 inches before the error exceeds 0.0015. It was found when set up at this distance that an unattenuated detector counting rate of 300/sec was obtained with a gas thickness such that the uncertainty in effective neutron energy was 9 kev. This geometry, shown in Fig. 1, was taken to represent the compromise sought.

B. Target Design

The greatest demand on the neutron source is that it be essentially monoenergetic, since no fast neutron detector combining reasonable sensitivity with high energy resolution is available for measurements in good geometry. For detailed knowledge of the spectrum of the neutron beam, one is therefore forced to depend upon an ion-beam calibration and the calculated kinetics of the primary reaction. In such a procedure, errors of the following four types are introduced.

(1) *Inaccuracy of accelerator energy.* Reliance was made upon the absolute voltage scale established by the Wisconsin group,[6] and to some extent, on the linearity and stability of an electrostatic deflector working on the diatomic beam.

(2) *Inaccuracy of target calibration.* By a proper choice of technique, this measurement can be referred to the same scale on which the incident energy is based.

(3) *Inaccuracy of Q value.*

(4) *Superfluous neutrons.* An uncertainty arises from neutrons differing in energy from forward neutrons produced in the primary reaction.

Errors of type (1) and (2) are small (Sec. II E), and the small Q value uncertainty can be reduced by future measurements. By far the most serious uncertainty is found in category (4). It is to be understood that here concern is with neutron sources that are wholly or partially shadowed by the scatterer (Fig. 2). The classification that has been adopted for the shadowed neutron components, measured as fractions of the total detectable flux, is as follows:

φ: forward d-d neutrons produced in the target gas ("primary flux").

γ_1: forward d-d neutrons produced in collimating apertures.

γ_2: forward d-d neutrons produced in end-wall of target.

ζ: neutrons produced in the primary reaction that scatter into the forward direction from the walls of the target structure. Since the angular variation of the energy in the d-d reaction at the beam energy used here is large, many of these scattered neutrons are of considerably lower energy than $\bar{E}_n$, the mean energy of the primary flux.

The source γ_1 is likely to be large in measurements with a deuteron beam. Carbon layers depositing on the apertures produce a broad distribution of low energy neutrons with high yield at our bombarding energy, and deuterium occluded in depth on these surfaces produces a distribution extending from about 3 Mev to the energy of the primary flux. The effective strength of this source has been maintained at a low value by means of the arrangement of collimators shown in Fig. 1 and by using a detector whose efficiency for the lower energies is relatively poor.

Neutrons γ_2 are the result of d-d interactions below the surface of the end wall in which the beam stops. The end wall was made of gold; a material of high atomic number was selected to reduce the possibility of producing (d,n) neutrons in the wall material itself. The mean energy of the γ_2 neutrons is estimated to be approximately 0.5 Mev less than the energy of the primary flux under the conditions of this experiment. The γ_1 and γ_2 sources, with attendant corrections, are discussed in Sec. II F.

In order to keep the strength ζ of the scattering in the target walls small, a thin-walled target was built as shown in Fig. 1. The outer wall of the target was machined from brass stock to a thickness of 0.005 inch on a diameter of $\frac{1}{2}$ inch and over a length of 4 inches. This wall thickness is computed to be close to the

[6] Herb, Snowdon, and Sala, Phys. Rev. 75, 246 (1949).

collapse limit of the target under one atmosphere pressure. The end wall was 0.006-inch gold foil, rim-soldered to a thin flange. A small gasket sealed the gas cylinder to an intermediate thin-walled (0.010-inch) section which supported the entrance foil and filling line. The entrance foil was of 0.00005-inch nickel mounted on an opening $\frac{1}{4}$ inch in diameter, and was required to withstand a pressure of 25 cm for bombardment times of the order of 50 hours at a maximum current of 2 microamperes. The section supporting the entrance foil in turn was sealed with an "0" ring to a heavier tube, on which the last two collimating apertures were mounted. The assembly was attached to the beam tube by means of Marman[7] clamp and flanges. The design is such that only thin walls subtend significant solid angles at the source. To prevent deuterons scattered in the entrance foil from striking the brass side wall of the target, a lining of 0.002-inch gold foil was used.

A particularly important feature of this target design is the foil mounting. In order to reduce the solid angle subtended by the gasketed flange at the neutron source, the foil was situated on a short re-entrant tube with 0.005-inch walls and end. The end was drilled to $\frac{1}{4}$-inch diameter, leaving a margin for mounting of about 0.090 inch. The foil could be waxed to this mount, but it was found that the temperature rise in foils under bombardment was too great to permit this unless a retaining ring was added, which, however, undesirably increased the mass. It was found that foils could be successfully soldered to the mounting, using the following technique. The mounting is warmed on a hot plate and covered with a thin layer of high-tin solder. The foil is cut oversize and laid on a clean aluminum surface that has been brought just above the solder point. The mounting is quickly inverted on the foil, and is lifted when solder begins to flow well. In almost every trial this procedure led to a good bond that outlived the foil itself.

The total wall scattering for the target was estimated on the basis of the known reaction kinetics, angular distribution of the *d-d* reaction, detector efficiency as a function of energy, and reasonable assumptions concerning the differential cross section for scattering of neutrons in the walls. Results of the calculation are shown in Fig. 3. The effect of this flux on the apparent cross section of polyethylene of transmission 0.50 has been calculated to be 0.03 percent.

C. Detection and Monitoring

The detector used in this experiment was of the recoil type consisting of a ZnS and Lucite molded detector[8] developed in this laboratory. The recoil unit was a cylinder one inch in diameter and $\frac{5}{8}$ inch high, mounted on an RCA type C 7151 experimental photomultiplier whose photocathode diameter is $1\frac{1}{4}$ inch and whose over-all diameter is $1\frac{1}{2}$ inch. This detector is comparatively insensitive to gamma-rays, has a short rise time and pulse duration, and has an efficiency of the order of one percent at the discriminator levels and neutron energy used in this experiment.

The response of the detector to primary neutrons and to background of types γ and δ (Sec. II F, G) is shown in Fig. 4. It is clear that the component δ, which includes photons and neutrons originating in the accelerator, is less than 1 percent of the total flux for all bias settings above 3 volts. At 15 volts, the lower of the two settings used, it contributes 0.2 percent. It also appears that the neutrons comprising γ are, on the average, slightly lower in energy than the primary beam, as expected. This was confirmed by measurements on the background and from transmission data taken on the γ component (Sec. II F).

Define as a rate effect any behavior of the detector system that produces observed counting rates not proportional to the incident flux over the range of rates involved in the transmission runs. Such an effect leads to a systematic error in transmissions measured in the conventional way, that is, from the ratio of attenuated to unattenuated counting rate at constant source intensity. If the effects are small, if n and n^0 denote the incident and observed counting rates, and if T and T^0 the true and observed transmissions, the unattenuated count can be written as

$$n^0=n(1+a_1n+a_2n^2+\cdots), \tag{4}$$

and the attenuated count as

$$T^0n^0=Tn(1+a_1Tn+a_2T^2n^2+\cdots). \tag{5}$$

From these definitions and the fact that

$$d\sigma/\sigma=(1/\ln T)(dT/T),$$

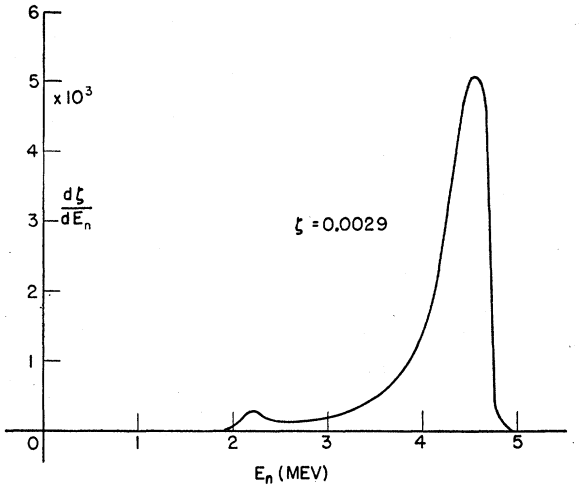

FIG. 3. Calculated differential energy spectrum of neutrons scattered into the forward beam by the walls of target shown in Fig. 1. Integration of the spectrum yields the value $\zeta=0.0029$. This flux raises the apparent cross section of a CH_2 scatterer of transmission 0.5 by less than 0.03 percent.

[7] Manufactured by Marman Products Company, Inc., Inglewood, California.

[8] W. F. Hornyak, Rev. Sci. Instr. **23**, 264 (1952).

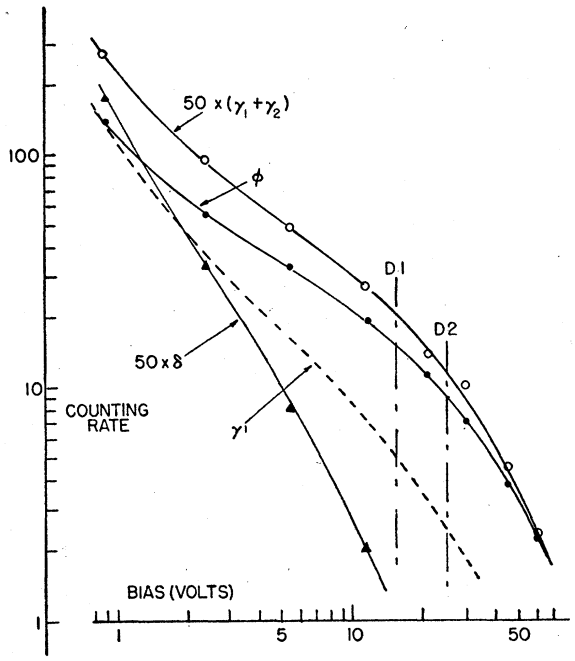

FIG. 4. Integral bias spectra of forward neutrons, φ is the spectrum of d-d neutrons of energy 4.75 Mev. ($\gamma_1+\gamma_2$) was taken with target at vacuum, δ with evacuated target shadowed. γ' is obtained by subtracting the full-energy spectrum from the slit spectrum, normalized for largest pulses, and suggests a low energy component at about 2 Mev. D1 and D2 are the settings on channels 1 and 2 in transmission measurements.

the shift in apparent cross section up to effects of second order is

$$\Delta\sigma/\sigma=-(1/\ln T)[a_1 n(1+a_1 n)(1-T)+a_2 n^2(1-T^2)]. \quad (6)$$

The effect is positive when the coefficients are positive.

The probability of superposition of two pulses of finite duration gives a shift whose magnitude and sign depend upon the pulse-height spectrum and operating bias. The effect is of first order. In Appendix I, a_1 is calculated as a function of bias for a spectrum closely resembling the observed curve, and it is shown that there is a setting for which the gain of counts due to pile-up of small pulses is compensated by loss of counts due to pile-up of large pulses. In this experiment one scaler was operated at this setting and the other at a bias such as to give approximately half as great a counting rate. It was therefore possible to look for significant discriminator and scaler rate effects by a comparison of transmissions taken on the two channels.

A total of about 2.6×10^7 unattenuated detector counts was taken on channel 1, at an average rate of 200 cps. The mean value of the quantity T_1/T_2 deduced from the data was found to be 1.00023 ± 0.00021, the probable error being computed externally from a treatment of the counting statistics of the measurements. The error computed internally from the deviations of 20 subgroupings of the data was 0.00019. This effect was considered to be not significant, and no correction has been made for it.

An additional check on rate effects was obtained by dividing the runs into two groups, one being taken at twice the incident beam current of the other. The two rates worked with were about 150 and 300 cps on channel 1. All cross sections were corrected as well as possible for other effects (Sec. III B). The analysis of about 75 runs at low flux and 100 at high flux, each run having 0.58 percent statistical accuracy, gave a mean value for the quantity $T_{\text{high}}/T_{\text{low}}$ of 1.0012 ± 0.0008. The probable error is statistical and is the same when computed externally and internally. An estimate of systematic error in the current dependence of background (Sec. IV) must be added to this error. The result is to raise the probable error to 0.0014. Since an effect larger than this was not uncovered in the data quoted above, no attempt has been made to correct the results.

Monitoring of the neutron source was accomplished by using a recoil unit of the same type as the detector but mounted on a 5819 phototube. The monitor saw neutrons at 90° to the incident deuteron beam and with such geometry that its counting rate increased by an amount calculated to be less than 0.03 percent due to backscattering from samples in the forward beam. As seen in the block diagram (Fig. 5), the detector and monitor systems were essentially identical. The non-overload feature of the detector amplifier was added in order to eliminate widening and to reduce overshoot and ringing of occasional large pulses. The total pulse duration (including a small overshoot) was observed to be less than 5 microseconds at the output of the amplifier. A Model 1030 (Atomic Instrument Company) scaler was used on detector channel 1 with a 1-microsecond resolving time. The remaining three scalars had 5-microsecond resolving times. The stability of this system against time and variation of ion current is shown in Fig. 6, which displays the first section of data taken on a polyethylene scatterer of transmission 0.523. The detector-to-monitor ratios on single runs, with scatterer out and in, are given for two pairings of the

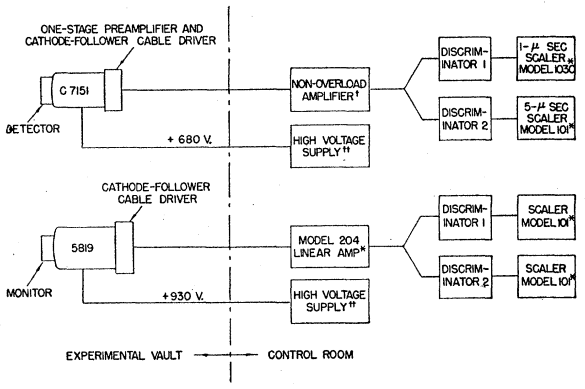

FIG. 5. Schematic of electronics. *Atomic Instrument Company; † Chase and Higinbotham, Rev. Sci. Instr. 23, 34 (1952); †† W. A. Higinbotham, Rev. Sci. Instr. 22, 429 (1951).

four channels used. The statistical probable errors of the runs, taken from the deviations, are approximately 1.5 times the error deduced from the number of counts, indicating that electronic jitter in these runs was competing with counting statistics. During subsequent measurements, the stability improved. Corresponding analysis of all runs (Sec. V) gave a ratio 1.1 of observed to computed statistical error.

The design of the detector preamplifier assembly deserves note. It was found in preliminary runs that unshadowed masses adjacent to the recoil unit can scatter a significant fraction of the neutron flux into the detector. Such an effect makes the background β a function of shadow diameter and position, and increases the uncertainty of its measurement. The difficulty was avoided with an in-line design such that the entire assembly was shadowed, with a safety margin, by scatterers of smallest diameter. Furthermore, in order to facilitate alignment of scatterer and detector, the axis of the assembly was kept open and a thin tube inserted from front to back. When the phototube was removed, the target and scatterer were visible and accurate alignment was easily accomplished.

D. Scatterers

In this experiment, scatterers of polyethylene $(CH_2)_n$ and graphite were used to determine cross sections which, upon appropriate subtraction, yielded the hydrogen cross section. Such measurements involve determinations of length, density, and deviations from purity of the scatterers. The extent to which uncertainties in the carbon cross section enter the determination of σ_H required that the accuracy of the constants for graphite samples had only to be about one-third of that for polyethylene.

Uncertainty of length measurement is a constant linear amount and sets an upper limit to transmissions that can be used. If an error of 0.0003 inch is not to produce an error in cross section greater than 0.05 percent, the minimum scatterer length is 0.6 inch, corresponding to a polyethylene transmission of 0.75. Consideration of statistical uncertainty in a measurement of reasonable duration sets a slightly lower transmission limit. A lower limit to transmission is set by the uncertainty of background measurement at 0.30 or a length of 2.5 inches. Polyethylene scatterers of these two limiting lengths were used, together with a set of three more at an intermediate length. Table I lists as l_0 the micrometer readings averaged over the proper central region of the scatterers, that is, the region that shadows the sensitive volume of the detector. Owing to imperfections in machining the scatterers, l_0 usually differed from the average lengths $\bar{l}$ taken over the entire scatterer. For graphite, l_0 was taken equal to $\bar{l}$. Diameters and vacuum weights are also listed in Table I.

Polyethylene may be expected to yield slightly under the pressure of a micrometer. This effect was checked by independent measurements of sample E, using an accurate shadow comparator and a Pratt-Whitney supermicrometer set to two pressures and extrapolated to zero. The results are shown in Table I. The values of $\bar{l}$, D, and M permit the density ρ_1 to be computed. The mean value for the five polyethylene samples is 0.9221 ± 0.0003 g/cm³.

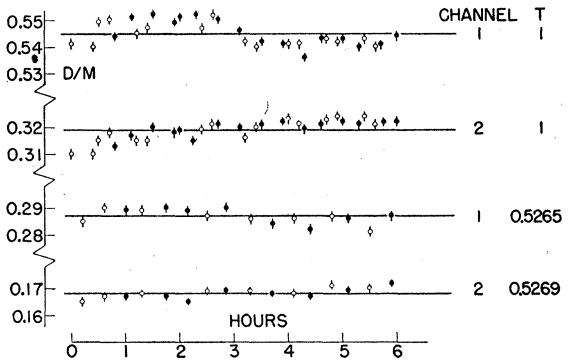

FIG. 6. Record of first six-hour run on the system of Fig. 5. Each point represents 64 000 counts in detector channel 1 and about half that number in channel 2. The two upper sets were obtained with no attenuation in the neutron beam; the lower two with scatterer B (Table I) in the beam. Open circles represent data taken at beam current 2.0 microamperes; solid circles at 1.0 microampere. The statistical probable error of the resulting transmission values is about 0.0010.

It was found that a more precise determination of density follows from measurement of buoyancy is distilled water, if care is taken to eliminate effects of surface tension, air bubbles, and failure of surfaces to wet. The results of this measurement, corrected to 22°C, are given in Table I as ρ_2. The mean value and temperature coefficient from the buoyancy method are

$$\rho_2=(0.9214\pm0.0001)(1-0.00065\Delta T)\ \text{g/cm}^3. \quad (7)$$

The discrepancy between density values by the two methods is somewhat outside probable error, and may indicate unknown systematic effects. In calculating the results, Eq. (7) has been applied.

It is clear from an inspection of Table I that the polyethylene is extremely homogeneous. It is well known, however, that bulk graphite is not, and that its density is considerably lower than that of the pure crystal (2.25 g/cm³). Thus, there is a need to estimate the effect of both microscopic and macroscopic inhomogeneities in the graphite on the cross-section determination.

Assuming that the process of compressing microcrystalline powder into graphite stock leaves spherical holes, all of equal radius r and randomly distributed through the sample, it can then be shown that an apparent cross section is lower than a true cross section by an amount

$$\frac{\Delta\sigma}{\sigma}=\frac{2}{3}\left(1-\frac{\sigma}{\rho_0}\right)\frac{r}{\lambda}, \quad (8)$$

where ρ is the observed bulk density, ρ_0 the crystalline

TABLE I. Properties of scatterers at 22°C.

Sample	Material	l (inches)	l_0 (inches)	D (inches)	M_{vac} (grams)	ρ_1 (g/cm³)	ρ_2 (g/cm³)	a (barns)
A	$(CH_2)_n$	0.9114	0.9119	1.2502	16.895	0.9214	0.9214	25.126
B	$(CH_2)_n$	1.3722	1.3719	1.2363	24.891	0.9220	0.9214	16.701
C	$(CH_2)_n$	1.3686	1.3680	1.6226	42.822	0.9228	0.9214	16.749
D	$(CH_2)_n$	1.3707	1.3683	1.9896	64.396	0.9220	0.9213	16.745
E	$(CH_2)_n$	2.5063[a]	2.5059	1.2057[b]	43.228	0.9223	0.9214	9.1432
F	C	2.0796		1.2519	72.177	1.721		5.052
G	C	2.0808		1.6247	121.911	1.725		5.034
H	C	2.0810		2.0005	184.855	1.727		5.028
J	C	4.0350		1.2519	141.267	1.736		2.578

[a] 2.5064 by shadow; 2.5066 by supermicrometer.

[b] 1.2056 by shadow.

density, and λ the mean free path for scattering in the actual bulk sample. For holes of radius 0.010 inch (considerably greater than the size of cavities visible on the surface), this effect is less than 0.1 percent. The effect therefore has been ignored in the results.

The macroscopic variation in density requires, however, that the number used in computing cross sections be the mean density over only the proper central region of the scatterer. Thus, at the completion of the runs, all graphite samples were machined to the diameter of that region and the densities remeasured. In most cases the change was negligible; the later values are listed as ρ_1 in Table I.

It is convenient to define for a given scatterer a constant a given by

$$a=\frac{A\ \ln 10}{Nl_0\rho}\times 10^{24}\ \text{barns}, \tag{9}$$

where N is Avogadro's number, A the molecular weight, and ρ the density. In obtaining the values listed in Table I, $N=6.0254\times 10^{23}$ was used, and the assumption was made that the scatterers are chemically perfect samples of CH_2 and C. ($A_{CH_2}=14.0317$; $A_C=12.0151$). Since a is proportional to D^2, a temperature correction amounting to $\frac{2}{3}$ of the polyethylene coefficient [Eq. (7)] must be applied. No temperature corrections were made for graphite. The constant then conveniently relates transmissions to cross sections through

$$\sigma=a\log_{10}(1/T)\ \text{barns}. \tag{10}$$

The polyethylene scatterers were machined from commercial[9] stock. A macrochemical analysis of this material by the Bureau of Standards has yielded the following analysis: percent by weight of H=14.37 $\pm$0.01, C=85.57$\pm$0.03, O=0.07$\pm$0.02, residue=0.007 $\pm$0.002. The oxygen content revealed here is consistent with the assumption that each polymer chain of approximate length equal to 1500 carbon atoms, as determined by infrared spectroscopy on one of these samples, is terminated by an oxygen atom.

[9] Plax Corporation, Hartford, Connecticut, who supplied the stock, fabricates it from pure bulk ethylene resin obtained from the Bakelite Company.

The net correction given by the chemistry to the hydrogen cross section, taking into account H, C, and O observed in polyethylene, is readily calculated to be -0.1 millibarn, and an upper limit for the effect of the residue to be -0.3 millibarn. The uncertainty introduced by the chemistry into the hydrogen cross section is 0.07 percent.

The graphite samples were cut from material of 99.98 percent purity, and unless the contaminants have cross sections exceeding 5 barns their effect on σ_C is negligible. The possibility that water is absorbed in this material has been removed by observing no loss of mass on baking.

The effects of neutrons scattered out by air displaced by the scatterers, and scattered in by the thin blades used to support the samples, have been estimated and found to be negligible.

E. Neutron Energy

The arguments connected with the significance and straightforward interpretation of the cross section (see Sec. I) have indicated a choice of energy close to 5 Mev. Consideration of the upper voltage limit of the electrostatic accelerator at this laboratory led to the $H^2(d,n)$-He^3 reaction with a gaseous target as the most convenient neutron source. The highest reliably attainable bombarding voltage of 1.8 Mev was used principally for the following reasons:

(1) It permits the most accurate determination of the energy loss of the deuteron beam in the target and entrance foil since this energy is closest to twice the proton energy at which sharp and intense resonances occur that are convenient for such calibrations.

(2) It gives the smallest energy loss for a fixed physical thickness of foil and gas.

(3) Finding that prior work on the scattering cross section of carbon is not quite detailed enough to reveal structure that would affect the measurements, careful runs through the usable neutron energy region were made, resulting in the data shown in Fig. 7. The energy region in the vicinity of 1.8 Mev is seen to be free from such structure.

(4) It was found that at 1.8 Mev, carbon gives the

smallest relative contribution to the cross section of polyethylene (refer Fig. 7).

(5) Backgrounds of type γ and δ increase with bombarding voltage, because of the relatively large thicknesses of the sources involved, and because C—d neutrons are more efficiently detected at higher energies. At voltages much above 1.8 Mev, these backgrounds become excessive.

The energy of the incident beam was thus chosen as 1800 kev. Electrostatic analysis of the D_2^+ beam was used for control and stabilization of the accelerator voltage. The energy scale was established, and linearity and stability checked, by adopting as standards[6] the values 873.5 kev for resonance in $F^{19}(p,\alpha\gamma)O^{16}$, 993.3 kev for resonance in $Al^{27}(p,\gamma)Si^{28}$, and 1882 kev for threshold in $Li^7(p,n)Be^7$. Many runs on these reactions have allowed us to arrive at a limit of uncertainty of 0.1 percent in the voltage scale. The assumption was made that a fixed analyzer voltage focuses D_2^+ and H_2^+ ions of exactly the same energy.

Forward neutrons produced in the target cover an interval of about 200 kev, due primarily to energy loss of deuterons in the gas. The knowledge of the functional form of the dependence of total n-p cross section on energy permits the definition of an effective mean neutron energy $\bar{E}_n$ in such a way that the observed cross section corresponds to neutrons of this energy alone.

The necessary accuracy in the target and foil energy losses can be achieved by making direct measurements on the energy loss of protons of approximately half the deuteron energy. Using the fact that deuterons and protons of equal velocities have equal rates of energy loss, the initial and final energies of deuterons in the gas were found with essentially the same precision as that obtained in the measurements of proton energy loss. The energy loss of protons was determined by measuring the mid-points of thick-target resonances after the proton beam had traversed the Ni foil alone, and the foil and gas combined.

When observed through the foil, the $Al^{27}(p,\gamma)Si^{28}$ resonance at 993.3 kev showed a width of about 20 kev, as compared with a width of 5 kev for measurements in the direct beam. A similar result was obtained with the fluorine resonance. The increase in width is much larger than the straggling and is probably due to nonuniformities in foil thickness. This width contributes the largest source of error to the energy-loss determinations. The reproducility of resonance mid-points suggests an error of 2 kev, but the possibility of a nonsymmetrical distribution of fluctuations in foil thickness increases the uncertainty to 4 kev.

Since the deuteron energy in the foil and gas was not exactly twice the proton resonance energies, extrapolations of the proton energy losses, amounting to approximately 15 percent, were necessary. They were made with the aid of the Bethe-Bloch formula with corrections for the K electrons,[10] using $I=300$ ev[11] as the ionization potential of Ni. It was thus determined, for example, that the deuteron energy loss in one of the two foils used in this experiment was 160.6 ± 4.6 kev, giving as the deuteron energy leaving the foil $1.639_4 \pm 0.005$ Mev.

Since the gas target thickness was known (i.e., length 8.14 ± 0.16 cm and 250 ± 1 mm Hg pressure), the resonance measurement on protons that had penetrated the foil and gas could be used to find the ionization potential for H_2 and D_2. The value obtained, including the C_k correction, is $I=20\pm2.5$ ev. A recent analysis by Bogaardt and Kondijs[12] of all range-energy data obtained with natural alpha-emitters yields $I=17.1\pm0.4$ ev, which is in agreement with the less accurate result obtained here. It was decided to use the value for I obtained here in calculating the deuteron energy loss, since it tends to remove certain systematic errors (in length and pressure measurements, for example) from the determination of mean deuteron energy. The energy loss in the gas thus obtained is $195._4\pm7$ kev, which results in a mean deuteron energy in the target of $\bar{E}_d=1.541_7\pm0.006$ Mev.

From the kinematics of the $H^2(d,n)He^3$ reaction including a small relativistic correction, and the Q value of 3.268 ± 0.004 Mev,[13] the corresponding mean neutron energy emitted in the forward direction is $\bar{E}_n=4.749 \pm0.009$ or $4.749(1\pm0.0019)$ Mev.

The energy dependence of the total n-p cross section is such that, at this energy, $\Delta\sigma/\sigma=-0.70\Delta E/E$. Therefore, the 0.19 percent uncertainty in $\bar{E}_n$ is equivalent to an uncertainty of 0.13 percent in the cross section.

It is necessary to consider three sets of effects that tend to make the mean neutron energy, as measured above, depart from the true effective mean neutron energy, defined as the single energy for which the total

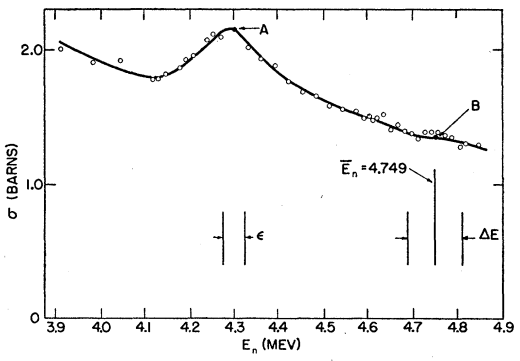

FIG. 7. Total cross section of carbon *vs* mean energy in a target of thickness ϵ. The target thickness and mean energy (ΔE and $\bar{E}_n$) used in the transmission runs are also shown. The solid points, A and B, have probable errors of about 0.5 percent.

[10] M. S. Livingston and H. A. Bethe, Revs. Modern Phys. **9**, 261 (1937).

[11] $I_{Ni}=(28/29)I_{Cu}$, where $I_{Cu}=310$ ev from R. Mather and E. Segrè, Phys. Rev. **84**, 191 (1951).

[12] M. Bogaardt and B. Kondijs, Physica **18**, 249 (1952).

[13] Whaling, Li, Fowler, and Lauritsen, Phys. Rev. **83**, 512 (1951).

n-p cross section is identical with the cross section observed with the finite energy width of the mean in the target. The effects are

(1) reduction of mean energy due to departure of the angle between the direction of an incident deuteron and the direction of the corresponding detectable neutron from zero.

(2) Shift of effective mean energy due to variation of σ_H over the energy interval, and to the variation of d-d yield and detector solid angle through the depth of the target.

(3) Corresponding shift due to resonance structure of σ_C within the interval.

An estimate from formulas[14] of the multiple Coulomb scattering of deuterons gives the rms angle of scattering in the Ni foil as about 2° and the angle in the D_2 gas as considerably less. The finite angle subtended by the recoil detector is less than 1°. These angular departures from zero produce a negligible reduction (i.e., 0.02 percent) in the mean neutron energy.

The effects grouped as (2) above produce an over-all effect which is of second order in the deviation of deuteron energy in the target from the mean energy. The linear terms drop out since they arise from an integration of an odd function over a symmetric interval. The numerical values indicate an effect of 3×10^{-5}, which can be neglected. The calculated effect is very small as a result of a fortuitous cancellation of terms. A conservative upper limit to the uncertainty resulting from error in the terms involved is 0.03 percent.

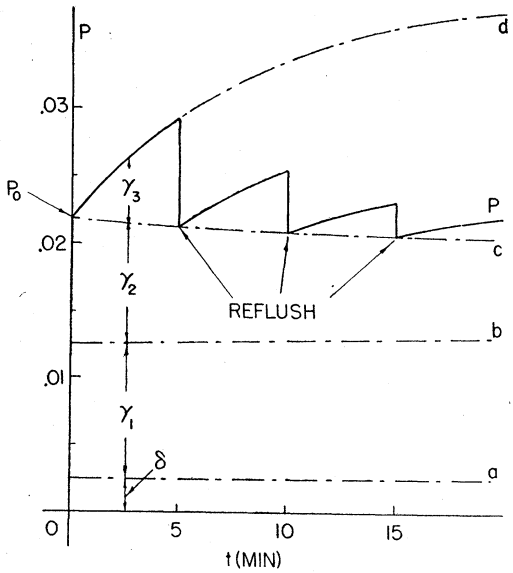

FIG. 8. Schematic short-time behavior of detector count with hydrogen filling, relative to count with deuterium filling. Deuterium is removed at time zero, and the solid curve p represents observed fluctuations of count for subsequent running and refilling cycles. The dashed curves represent the components believed to contribute to p (see text).

[14] W. T. Scott, Phys. Rev. 85, 245 (1952).

A similar calculation has been carried out in order to estimate the shift due to possible resonance structure in the carbon cross section. The effect is again of second order in the relative energy deviation, and it has been found that any structure consistent with the data of Fig. 7 produces a negligible shift in cross section. The observed hydrogen cross section is therefore essentially identical with the cross section for a hypothetical homogeneous neutron beam of energy $\bar{E}_n$.

F. Hydrogen Background

For the purposes of this discussion, background is defined as any component of the unattenuated neutron flux that does not originate in the d-d reaction in the gas volume of the target, or, if it does so originate, does not pass without scattering into the detector. Referring, then, to Fig. 2, one sees that the total flux consists of the primary component φ and three essentially distinct types of background. Neutrons ζ, which arise from target-wall scattering of d-d neutrons, were considered in Sec. II B, where it was shown that the cross section shift resulting from them is negligible. Neutrons β are the result of scattering from the room walls and other remote masses, and are discussed in Sec. II G. Concern here is with the components γ_1 and γ_2 produced in beam-defining apertures and the Au end wall of the target, respectively. These neutrons have a significantly lower mean energy than the primary neutrons and, since they are produced on the axis of the experiment, are geometrically indistinguishable from them. In Appendix II it is shown that

$$T=T^0+(\gamma_1+\gamma_2)(T-T_{12})-(1-T)\beta, \qquad (11)$$

where T is the true transmission of a given scatterer for the component φ, and T_{12} is its transmission for the components γ_1 and γ_2 combined. In order to make the correction for this background, both its magnitude and its transmission must be known.

Direct measurements of the necessary quantities are in principle possible when D_2 in the target is completely replaced by H_2 at the same pressure. Under this condition the deuteron beam current and energy at all surfaces in question are exactly reproduced. After subtraction of shadow background (Sec. II G), the unattenuated counting rate (relative to the rate with deuterium filling) gives $(\gamma_1+\gamma_2)$, and the rate with scatterer in gives T_{12}.

Experience showed that this procedure must be examined more carefully. It was found that a significant rate of ion exchange occurred at the walls of the target during bombardment, so that deuterium which had been occluded during previous running reappeared in the target volume during hydrogen runs. Also, the strength of γ_2 was found to diminish slowly during hydrogen runs, again as the result of the diffusion of deuterium out of the Au surface into the gas. The time-dependence of the detector count, as observed in many runs, is shown schematically in Fig. 8. The shadow count

δ is very steady at 0.0025. The count at time zero, which is called p_0, is the sum $(\delta+\gamma_1+\gamma_2)$ and is assumed to represent the state of the system in the deuterium runs just preceding the hydrogen background run. After a few minutes of running, the exchange of hydrogen with deuterium in the target walls has released an amount of deuterium gas producing the component γ_3; these neutrons are presumably of the same energy as the primary neutrons φ, and therefore correspond to transmission T. A complete reflushing of the target with H_2 removes this D_2 fraction and reduces the count rate, which then builds up again as more gas is exchanged, and subsequent flushings finally remove most of the D_2. Meanwhile, the component γ_2 is steadily falling as the end wall exchanges gas, and γ_1 is rising very slowly as carbon and deuterium continue to build up on apertures in the beam. The net effect of these two drifts is to make the initial count after successive flushings diminish until all the D_2 has been lost from the end wall. Bombardment of the Ni window does not contribute to γ_1 or γ_2, presumably because it runs too hot to retain contamination layers.

Although the details of this picture of the hydrogen background are not essential to a proper correction, it is of interest to note that they have been confirmed by many observations. It was found, for instance, that when the target after running with deuterium was evacuated and then sealed off, the variations of γ_2 and γ_3 under continued bombardment disappeared, and that the target pressure did not rise, thus indicating that the appearance of D_2 during hydrogen runs was the result of exchange and not simply of outgassing due to warm-up. Cleaning apertures and replacing the target end wall with fresh gold reduced p_0 in the expected way, and an inverse-square study of $(\gamma_1+\gamma_2)$ as a function of detector distance showed that γ_1 came mostly from collimators 2 and 3 (Fig. 1). The long-time behavior of p_0, which is shown in Fig. 9, is also understandable. The slits started clean at time zero. During the first 47 hours of beam time the hydrogen runs were brief (20–30 min), and $(\gamma_1+\gamma_2)$ rose steadily to 0.028. At this point an extended H_2 run of 310 min removed most of γ_2, giving $\gamma_1\sim0.015$ and $\gamma_2\sim0.013$ at about 50 hours. At 83 hours collimators 2 and 3 were cleaned, removing most of γ_1. The subsequent low count indicated that just before cleaning γ_1 had risen to 0.022, and that γ_2 had again built up to 0.014 in the second half of the runs. It is therefore clear that the two components grow at about equal rates.

Finally it should be noted that, in addition to measuring p_0 directly, one can deduce it from measurements in the presence of γ_3. From the discussion of Appendix II, it is seen that

$$p(T-T_p^0)=(\gamma_1+\gamma_2)(T-T_{12})-(1-T)\delta, \quad (12)$$

where p is the entire hydrogen background count $(\delta+\gamma_1+\gamma_2+\gamma_3)$, and T_p^0 is the uncorrected in-out ratio for the given scatterer in this flux. The fact that

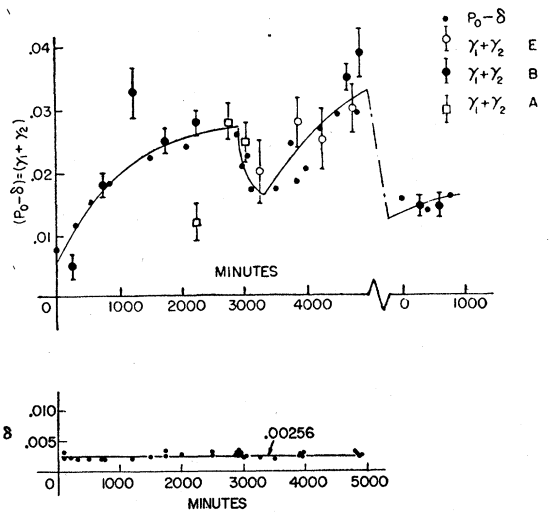

FIG. 9. Observed long-time variation of hydrogen backgrounds $(\gamma_1+\gamma_2)$ and δ, covering period of transmission measurements. The measurements are relative to count with deuterium filling. Time is taken as minutes of beam after cleaning aperture surfaces. The points labeled $(p_0-\delta)$ are the directly observed initial count (Fig. 8); other points are deduced through Eq. (12) from transmission measurements on scatterers *A*, *B*, *E*. These are somewhat less precise than the direct measurements, which are used to determine the curve. The dip at 3000 minutes is the result of extended running with hydrogen filling, which replaces deuterium in end-wall of target. δ is the corresponding shadow background. Since its source is within the accelerator, where the accumulation of carbon and deuterium layers has been progressing for a much longer time, the background is expected to be constant over this interval.

$(\gamma_1+\gamma_2)$ is essentially constant during a hydrogen run implies then that, as p rises rapidly due to the growth of γ_3, T_p^0 must approach T at such a rate as to maintain invariance of the product $p(T-T_p^0)$. Use has been made of Eq. (12) to compute $(\gamma_1+\gamma_2)$ from measurements of T_p^0 as a check against the direct measurements of p_0, and the points are shown in Fig. 9. The agreement between the background deduced by this method, and p_0 as directly measured, is good. The transmissions T_{12} (Table II) needed here and in Eq. (11) were obtained from poor-geometry high rate measurements with the target at vacuum. It was assumed that the energy distribution of γ_1 and γ_2, and hence of T_{12} for a given scatterer, were independent of time. Now the measured background would be expected to be an upper limit to p_0, since γ_3 may not be exactly zero; on the other hand, values of $(\gamma_1+\gamma_2)$ deduced through Eq. (12) should represent a lower limit, since the end wall tends to lose deuterium during the measurement. Thus, the agreement between the two methods lends confidence to the belief that this background has been correctly treated.

It is interesting to attempt to describe the transmission of scatterers, with hydrogen filling, in terms of the observed integral bias spectrum of the neutrons involved (Fig. 4). It is assumed that the spectrum can be approximated by two groups, one just below the energy of the primary neutrons and the other at con-

TABLE II. Observed transmissions with hydrogen filling.

Sample	Material	T	T_{12}
A	CH_2	0.6509	0.575±0.012
B	CH_2	0.5225	01441±0.003
E	CH_2	0.3053	0.230±0.005
J	C	0.300	0.214±0.005

siderably lower energy. This grouping of energies is to be expected if the neutrons arise from *d-d* and C-*d* sources in the slit and end-wall surfaces. If the relative strengths of higher and lower energy groups is taken to be about 3-to-1, as suggested by the spectra, the calculated behavior of the transmission data can be shown to be in agreement with the data of Table II.

G. Shadow Background

The neutron component to be discussed here consists of the flux entering the detector along paths that do not traverse the scatterer; it is denoted by β (Fig. 2) and is measured in units of the total unattenuated count rate with deuterium filling. From Eq. (11) one sees that, for this component alone,

$$T=T^0-(1-T)\beta, \tag{13}$$

where T^0 is the observed in-out ratio for a scatterer whose true transmission of the direct beam is T. For proper correction of observed transmissions, β must be accurately known in magnitude; its spectrum is of no importance.

The background β was measured by using nickel shadows 10 inches long with a computed transmission of 0.0003. This value was based on a transmission measurement which gave 3.07±0.03 cm as the mean free path for the neutron energy used in this experiment. It was assumed that the computed shadow transmission is in error due to multiple scattering by no more than its full value. The shadows were cylinders of $1\frac{1}{4}$ and 2 inches in diameter to match the smallest and largest scatterers. No measurable diameter dependence of β was found, but nevertheless, the shadow geometry of Fig. 1 was used under the assumption that extension of source diameter (owing to production and scattering at points near the axis of the experiment) was more likely than corresponding extension of the detector, since all masses near the detector were known to be completely shadowed. This choice of geometry minimizes the difference between the flux attenuated by the scatterer and the flux removed by its shadow.

Most of the neutrons involved in the shadow background originate in the target and scatter from the walls and floor of the room. The small remainder, denoted by δ, come directly and by wall scattering from the accelerator, 19 feet or more ahead of the target. δ was measured frequently throughout our runs by means of shadow measurements with hydrogen filling. These data are given in Fig. 9, where it is seen that δ was essentially constant at 0.0025 through the experiment. This is to be expected, since the sources giving rise to it have been building up to their present thicknesses over a period of years.

Since β is normalized to the primary flux φ, the component of β originating in the target is independent of ion current. On the other hand, since the sources of δ are approximately independent of focus and deflection conditions, the counting *rate* of these neutrons is constant, and δ is therefore inversely proportional to the ion current. This accounts for the fact that β, measured as a function of ion current (Fig. 10), is a good fit to the curve

$$\beta=0.0127+0.0024/\bar{I}, \tag{14}$$

where $\bar{I}$ is the average ion current, in microamperes, reaching the target gas. As a result, the values of β to be used for correcting data taken at the high and low currents of the transmission runs differed by 0.0010.

H. Scattering-In Problems

In a measurement with finite geometry, a fraction of the attenuated count is attributable to neutrons that are detected in spite of having undergone one or more scatterings in the sample. This effect is called the "scattering-in." The first-order effect of scattering-in, due to single scattering, for a scatterer centered on the axis of the measurement, is

$$\Delta\sigma/\sigma=-fG, \tag{15}$$

where f is the anisotropy parameter defined in Eq. (2), and $G=(D/L)^2$. Denoting by f_h, f_c, and f_p the values of f for H, C, and CH_2, respectively, at the mean neutron energy $\bar{E}_n$, it is then easily shown that

$$f_h\sigma_H=\tfrac{1}{2}(f_p\sigma_p-f_c\sigma_c), \tag{16}$$

and that

$$\sigma_H=(\sigma_p{}^0-\sigma_c{}^0)/[2(1-f_hG)], \tag{17}$$

where $\sigma_p{}^0$ and $\sigma_c{}^0$ are observed cross sections, uncorrected for the effect, for CH_2 and C scatterers of equal diameter D. For isotropic *n-p* scattering in center-of-mass coordinates, $f_h=4$. Consequently, Eq. (17) gives the true cross section, corrected for single scattering, in terms of known or measured quantities, without requiring knowledge of f_p or f_c. Note that, since the length of scatterer does not enter Eq. (15), the choice of transmissions of CH_2 and C is immaterial.

A number of estimates based on various models for the scatterers indicated that the contribution of multiple scattering to the scattered-in flux is less than $\frac{1}{5}$ of the single scattering effect. Thus, the error arising from multiple scattering for the smallest diameter scatterer, where the total effect is 0.60 percent, cannot exceed 0.12 percent.

Both the length and the diameter of the polyethylene scatterers were varied in this experiment to establish the freedom from multiple scattering error suggested above. The five scatterers of Table I were made to

dimensions that would give scattering-in effects from 0.006 to 0.015 at transmissions from 0.30 to 0.65.

One criterion for freedom of the method from an uncertainty due to multiple scattering is given by the internal consistency of two computed cross sections: one obtained by extrapolating the diameter function, the other from the slope of $\ln T$ *vs* l_0. The results of this study are shown in Fig. 11. The cross sections deduced from them are $\sigma_p=4.734\pm0.003$ (diameter extrapolation) and $\sigma_p=4.728\pm0.003$ (transmission slope), where only the statistical probable errors are given. The conclusion drawn from this test is that multiple scattering does not produce effects greater than 0.12 percent in cross sections deduced from transmission measurements carried out in the geometry of this experiment.

III. DESCRIPTION OF RUNS

A. Schedule of Runs

The runs were scheduled for convenience in counting, the scaler on channel D1 being used to start the entire system and to stop it after a predetermined register count. Each run consisted of 64 000 counts unattenuated, followed by the same number with scatterer in, and finally by another out count of the same number. This in-out distribution is found to correspond closely to the most effective use of a given total time interval considering the statistics, background, and the range of scatterer transmissions. Such an optimization of time is desirable primarily to minimize electronic drift and time dependence of background. Runs at low beam current were alternated with runs at high current for a number of runs sufficient to give statistical significance to the pile-up study. A total of 209 runs were made on the CH_2 and C samples of Table I. Shadow and hydrogen background were measured frequently, and foil thicknesses checked for stability several times. Again from the standpoint of optimizing the use of the time, about one-quarter of the total time was devoted to the graphite measurements.

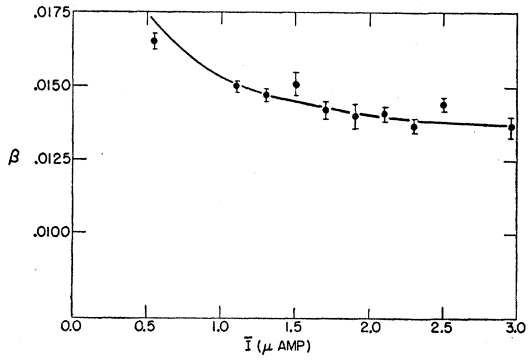

FIG. 10. Dependence of shadow background, measured with deuterium filling and normalized to the unattenuated flux, on average ion current at target. The rise at low current arises from the contribution of δ (see text), and fits Eq. (14), plotted here as the solid line.

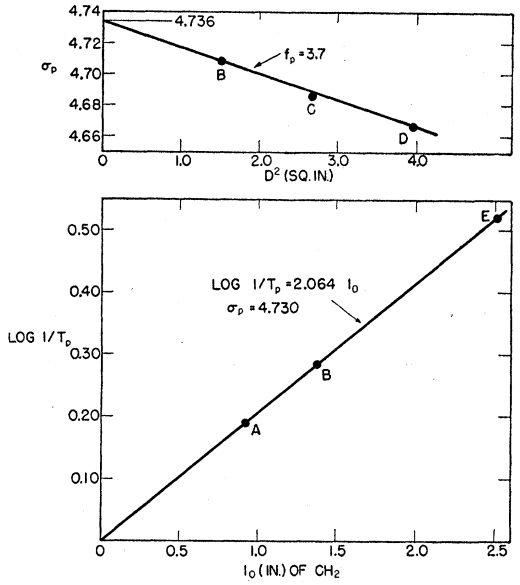

FIG. 11. Internal consistency check against multiple scattering-in, using diameter and length variation of polyethylene. The best line through the diameter plot is taken without regard to the f-value of hydrogen, and the scattering-in effect thus observed for scatterer B is used for A, B, and E in the second plot. The cross section obtained from the best fit (including the origin) of the length function is found to agree with the extrapolation of the diameter function to within 0.12 percent.

B. Computations and Corrections

For each run, the D/M ratio (detector count relative to monitor count) with scatterer in was divided by the average of the two unattenuated D/M ratios to give T°, the uncorrected transmission. There were two such values from each run, derived from the two pairs of channels in the detection system (Fig. 5). The results from channel 2 were used only to show that, over the experiment as a whole, there was no significant deviation of T_2^0/T_1^0 from unity and hence no significant rate effect; all final cross sections were then deduced from the data obtained from channel 1 alone.

The shadow background correction was made to T^0 by using Eq. (11) and the curve of Fig. 10, read at the appropriate beam current. The hydrogen background correction was made, also using Eq. (11), from the T_{12} data of Table II and the curve of Fig. 9, read at the appropriate time. The a values of Table I were then used (after temperature correction) with Eq. (10) to give σ^0, the cross section uncorrected for scattering-in.

The entrance foil of the target had to be changed about halfway through the experiment, after 42 hours of beam time; and the second foil was found to be several kilovolts thinner than the first. The difference was accounted for by a small correction to all the later cross sections using the known energy dependences of C and H. Thus, all data refer to a mean neutron energy of 4.749 Mev computed for the first foil.

Finally, a scattering-in correction was applied to each value of σ^0 in order to provide sets of completely cor-

rected cross sections for studies of internal consistency. These corrections were derived from f_p and f_c values obtained from best fits to the polyethylene and graphite diameter studies consistent with the value $f_h=4$, as discussed in Sec. V.

IV. SOURCES OF ERROR

The discussion of this section evaluates the contributions to the total probable error of the n-p cross section from all significant sources of which we are aware. We shall consider two sets of estimates; the first in most cases is based on observations of the stability of measurements, while the second is our opinion regarding the extent to which additional systematic errors may have entered the data. In some cases, the second value contains only the systematic estimate; in others, this estimate is combined with the first, as the square root of the sum of squares.

Table III lists twelve sources of error with the two sets of estimates of their magnitudes, given in parts per thousand of hydrogen cross section. The errors in hydrogen background correction are given, first, by the statistics of p_0 and T_{12} measurements (Fig. 9 and Table II) and, second, by combining with this an estimate of uncertainty due to loss and exchange of deuterium in the target end wall during the hydrogen runs. The estimate follows from the observation that the duration of a single run was at most 70 min, while the drop in p_0 indicated in Fig. 9 required bombardment for 220 min. The probable error from rate effects is given as the full effect observed by comparison of data at high and low beam current. The error in neutron energy contains an uncertainty of 4 kev in the Q value[13] of the primary reaction; the remainder, in the first estimate, includes the errors in target length and the fluctuations in resonance mid-points in successive foil calibrations. The second estimate takes into account the possibility that non-uniformities of the entrance foil produce asymmetries in the resonance data. The contribution of counting statistics in measurements of T^0 is given; the first estimate is the error for the experiment as a whole, and the second is the error for any one of the scatterer geometries taken alone. The statistical error in shadow background is deduced from the data shown in Fig. 10, while the second estimate allows for systematic uncertainties in this measurement of $\frac{1}{10}$ of its full value. The uncertainty due to multiple scattering is taken from the transmission-diameter inconsistency (Sec. II H); this is covered by the second estimate which is taken as $\frac{1}{5}$ of the full scattering-in effect for the smallest diameter scatterer. Observations on the limitations of the line-up procedure were used to deduce the error due to axial misalignment of scatterers. The uncertainty in composition of the polyethylene is taken from the chemist's quotations (Sec. II D). The error in scatterer dimensions is taken from the data pertinent to Table I, and the temperature of the polyethylene samples is assumed to be uncertain by 1°C. The effect of degradation by wall scattering is taken as the full computed effect. Finally, an estimate of the effect of the finite interval in neutron energy is included, taking into account all effects discussed in Sec. II E. In each of the two over-all estimates, the total error is taken as the square root of the sum of squares.

TABLE III. Breakdown of the total probable error (parts/1000).

Source	First	Second
H_2 background	0.5	2.1
Rate effects	1.5	1.5
Neutron energy	1.3	1.4
Counting statistics	0.7	1.4
Shadow background	0.4	1.3
Multiple scattering	1.2	1.2
Misalignment	1.0	1.0
Chemistry of CH_2	0.7	0.7
Dimensions	0.4	0.4
Temperature of CH_2	0.3	0.3
Degradation	0.3	0.3
Finite energy interval	0.1	0.1
Total	2.8	3.9

An inspection of Table III shows that in this experiment there are seven effects contributing approximately the same magnitude of error, and hence any attempt to reduce significantly the total error of 0.39 percent would necessitate improvements in most of these factors.

Since the purpose of the experiment is to obtain knowledge of the singlet potential, it is necessary to combine the total probable error of the cross-section measurement with the errors in other measured quantities entering the relation between cross section and the singlet parameters. The situation is at present such that the uncertainties in other experiments (see Sec. V B) correspond to a cross-section uncertainty of 0.3 percent. Thus, if the other parameters are treated as exact, the probable error of this determination must be increased to 0.5 percent. Note that a significant improvement in the precision of the cross-section measurement must be accompanied by better data on other parameters if the singlet parameters are to be more closely defined.

V. EXPERIMENTAL RESULTS AND INTERPRETATION

A. Examination of Cross-Section Data

The final cross sections of all scatterers, computed and corrected according to the procedures of Sec. III B, are given in Table IV. The scatterers are listed as in Table I; their transmissions and diameters are given here as nominal values. The column σ^0 represents cross sections corrected for shadow background, hydrogen background, temperature, and variation of foil thickness, but not for scattering-in effects. A best value for the hydrogen cross section, corrected for scattering-in, can now be computed, if it be assumed that multiple scattering can be ignored and that the n-p scattering

TABLE IV. Final cross sections for all scatterers.

Scatterer	Material	T	D (in)	σ^0 (barns)	σ (barns)
A	CH_2	0.65	1.25	4.686	4.713
B	CH_2	0.52	1.25	4.702	4.728
B	CH_2	0.52	1.25	4.715	4.741
C	CH_2	0.52	1.63	4.687	4.732
D	CH_2	0.52	2.00	4.667	4.735
E	CH_2	0.30	1.25	4.707	4.731
$(CH_2)_{Av}$					4.730±0.007
F	C	0.54	1.25	1.349	1.355
G	C	0.54	1.63	1.339	1.350
H	C	0.54	2.00	1.332	1.348
J	C	0.30	1.25	1.339	1.345
$(C)_{Av}$					1.350±0.003
A, B, E, F, J	H		1.25	1.679	1.689
C, G	H		1.63	1.674	1.691
D, H	H		2.00	1.667	1.693
$(H)_{Av}$					1.690±0.003

is isotropic. At each of the three scatterer diameters, σ^0 for hydrogen is obtained by subtraction of graphite from polyethylene, the weight of each value being determined by the number of runs taken at that diameter. For example, σ^0 for hydrogen at diameter 1.25 inch is half the difference between the mean of A, B, and E and the mean of F and J, and has four times the weight of the other two diameters. The three values thus obtained are fitted by least squares to the function $\sigma^0=\sigma(1-0.00384D^2)$, which takes into account the first-order scattering-in effect in the geometry of this experiment, with $f_h=4$. As pointed out in Sec. II H, this treatment does not require knowledge of f_p and f_c. It yields 1.690 barns for the corrected cross section of hydrogen, which we adopt as our final value.

The data can be examined from several distinct points of view, each of which tends to provide a test of internal consistency of the results. Such a test has already been described in connection with multiple scattering (Sec. II H), where it was pointed out that the best fit to the diameter function is consistent, to about 0.1 percent, with the best fit to the transmission function. It is appropriate to point out that certain systematic effects other than multiple scattering would also be expected to show up in this comparison. The background corrections fall into this class, since they are functions of transmission, Eq. (11). According to Eq. (6), pile-up is also expected to vary with transmission, as would the effect of a significant amount of low energy flux not accounted for by the hydrogen background correction.

A second consistency test is given by the statistical behavior of the results. For this purpose, fully corrected cross sections are obtained from σ^0 values by deducing the most probable scattering-in corrections for polyethylene and graphite. This is done by fitting the σ^0 data of Table IV to linear functions of D^2 that are consistent with $f_h=4$. The corrected cross sections are then listed as σ in Table IV. Each entry in the polyethylene data of this table represents the mean of a number of runs sufficient to give a probable error of 0.006 barn due to counting statistics; each graphite entry has a corresponding error of 0.003 barn. The mean values $(CH_2)_{Av}$ and $(C)_{Av}$ in Table IV are given with probable errors computed, for *any one* of the entries, from the observed deviations of single values. These are then reflected as an error of 0.003 barn in the n-p cross section $(H)_{Av}$. The agreement between observed statistical error and prediction from number of counts indicates consistency of cross sections over the range of transmissions and diameters used in the experiment.

Temperature drift, fluctuation of backgrounds, changes in foil thickness and accelerator calibration, and other slow time variations, are expected to show up in a time-sequential breakdown of corrected cross sections. All of the runs on polyethylene are studied in this way in Fig. 12, each point representing the mean of eight consecutive runs. The total probable error, estimated as in Table III, is also shown. Since corrections were made from smoothed data, the fluctuations of these points should reveal whatever significant effects are superimposed on counting statistics. The external probable error of the mean in Fig. 12, computed from the number of counts, is 0.0023 barn; the observed internal error is 0.0026 barn. The points are therefore consistent with a constant cross section of 4.730 barns.

Finally, the distribution of the errors of individual runs on polyethylene is compared with the normal distribution. In Fig. 13 integral plots are made for the three transmissions separately, and a differential plot for the entire set normalized to transmission 0.52. Agreement with normal distributions is satisfactory. Recalling the two tests against rate effects in the detector, described in Sec. II C, we have given a total of five checks against systematic errors of certain types. If no other errors have entered the measurement, the first estimate of Table III applies, and the probable error of the hydrogen cross section is 0.004_7 barn. Adopting the second estimate, we have the final value $1.690\pm0.006_6$ barns.

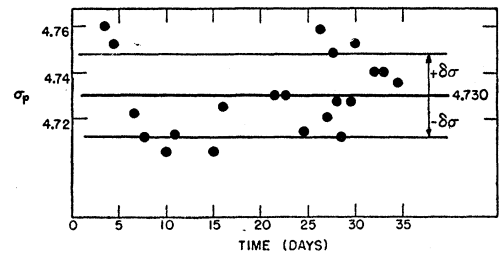

FIG. 12. Sequential breakdown of polyethylene cross sections, including all corrections, showing statistical consistency with a constant cross section. $\delta\sigma$ is the total probable error for polyethylene analogous to the error for hydrogen deduced from Table III.

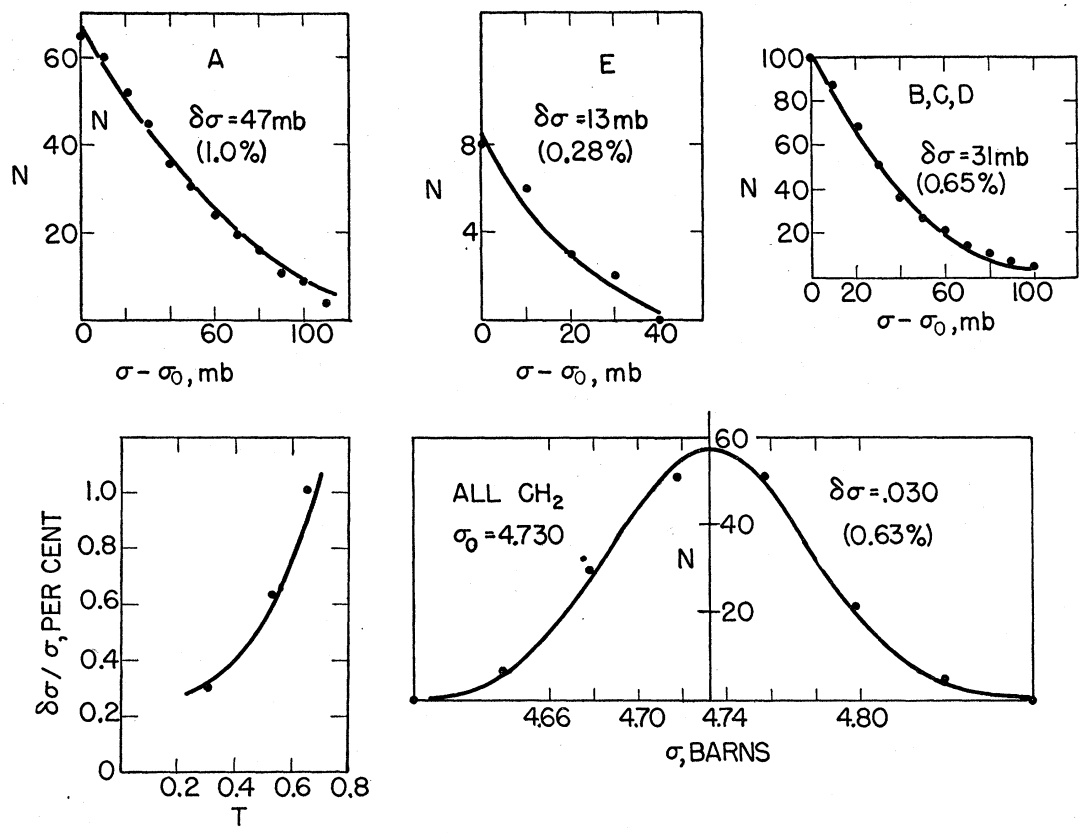

FIG. 13. Distributions of deviations of corrected individual runs on polyethylene around the mean value 4.730 barns. The three upper curves are integral plots for single transmissions compared with integrals of Gaussian functions (solid curves). The points on the lower left plot are the statistical probable errors per run at each transmission, read from the upper curves and compared with the prediction from counting statistics (solid curve). The final curve is the differential distribution of all runs, normalized to transmission 0.52, where the predicted statistical probable error per run is 0.58 percent.

B. Interpretation

From the theory of effective range,[1–3] the total n-p scattering cross section for angular momentum $l=0$ can be written

$$\sigma=\sigma_t+\sigma_s=\frac{3\pi}{k^2+[1/a_t-\frac{1}{2}\rho_t(0,E)k^2]^2}+\frac{\pi}{k^2+[1/a_s-\frac{1}{2}\rho_s(0,E)k^2]^2}, \quad (18)$$

where $k^2=ME/2\hbar^2$, and E=energy of incident neutron in the laboratory system. The subscripts t and s denote triplet and singlet states, respectively. In this notation,

$$\rho_t(0,E)\cong r_{0t}[1-2P_t r_{0t}^2k^2];$$

a_t=triplet scattering amplitude at zero energy;
r_{0t}=triplet effective range at zero energy;
P_t=small coefficient that depends on the shape of the triplet potential well. Such coefficients are tabulated in reference 2 as a function of (r_0/a).

The singlet parameters are defined analogously.

The contributions of higher angular momenta to the total n-p cross section are negligible below 5 Mev, so that σ of Eq. (18) represents the experimental total scattering cross section.

From measurements of the binding energy of the deuteron,[13] the epithermal n-p total cross section,[15] and the coherent scattering amplitude,[16] the three parameters a_t, a_s, and $\rho_t(0,-\epsilon)$ are determined:[17]

$$\begin{aligned} a_t&=5.378(1\pm0.0039)\times10^{-13}\text{ cm},\\ a_s&=-23.69(1\pm0.0024)\times10^{-13}\text{ cm},\\ \rho_t(0,-\epsilon)&=r_{0t}(1+2P_t\gamma^2r_{0t}^2)\\ &=1.702(1\pm0.017)\times10^{-13}\text{ cm}, \end{aligned} \quad (19)$$

where $\gamma^2=M\epsilon/\hbar^2$, ϵ=binding energy of the deuteron.

In the shape independent approximation ($P_t=P_s=0$), the total n-p cross section, $\sigma^{(S.I.)}$, is a function of the one unknown r_{0s} for a given energy. A plot of $\sigma^{(S.I.)}$

[15] E. Melkonian, Phys. Rev. **76**, 1744 (1949).
[16] Burgy, Ringo, and Hughes, Phys. Rev. **84**, 1160 (1951).
[17] For a list of the experimental values used, together with a discussion of the contributions of their experimental errors to the uncertainties in a_t, a_s, and $\rho_t(0,-\epsilon)$, see G. Snow, Phys. Rev. **87**, 21 (1952).

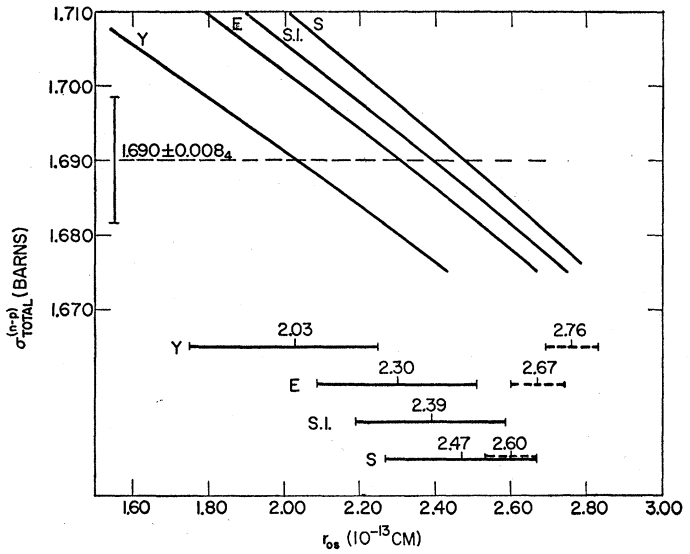

FIG. 14. Theoretical total n-p cross sections as a function of effective singlet range r_{0s} for the well shapes: Square (S), "Shape Independent" (S.I.), Exponential (E), and Yukawa (Y). Resultant values of $r_{0s}^{(n-p)}$ are shown and compared with $r_{0s}^{(p-p)}$ for each well shape.

versus r_{0s} at $E_n=4.749$ Mev, using the parameters of Eq. (19), yields $r_{0s}^{(S.I.)}=(2.39\pm0.20)\times10^{-13}$ cm for $\sigma=1.690\pm0.008_4$b.[18] This is illustrated in Fig. 14.

To consider shape dependent effects, we have plotted σ *versus* r_{0s} in Fig. 14 for the three potential well shapes: square (S), exponential (E), and Yukawa (Y). For simplicity we have assumed the same well shape for singlet and triplet potentials. The experimental result for σ then determines r_{0s} for each well shape, as shown in Fig. 14, and listed in Table V. In all cases σ is quite insensitive to r_{0s}; $(r_{0s}/\sigma)(\partial\sigma/\partial r_{0s})\simeq1/18$. Nevertheless, the experimental error in σ yields an uncertainty in r_{0s} for each shape that is smaller than or comparable to the differences between the values of r_{0s} for different shapes. Therefore, this experiment yields information about the singlet effective range coupled with the potential shape.

In Table V and Fig. 14, the values[19] of the proton-proton effective singlet range $r_{0s}^{(p-p)}$ are listed and compared with $r_{0s}^{(n-p)}$ for each potential well shape. The following results are found: for a Yukawa well, $r_{0s}^{(n-p)}$ is definitely smaller than $r_{0s}^{(p-p)}$; for an exponential well, $r_{0s}^{(n-p)}$ is smaller than $r_{0s}^{(p-p)}$ with errors that almost overlap; and for a square well, $r_{0s}^{(n-p)}$ is slightly smaller than $r_{0s}^{(p-p)}$ with errors that completely overlap.

A more rigorous test of the hypothesis of charge independence than the comparison of the quantities $r_{0s}^{(n-p)}$ and $r_{0s}^{(p-p)}$ is the comparison of the corresponding values of the singlet intrinsic range b_s defined by Blatt and Jackson.[20] The parameters b_s are more appropriate than r_{0s} since they characterize the range of the specifically nuclear potential, excluding the Coulomb potential. The values of $b_s^{(n-p)}$ obtained from this experiment are listed in Table V along with the more accurate values of $b_s^{(p-p)}$. The same conclusion follows from the comparison of b_s as for r_{0s}. Hence, a square well is compatible with charge independence, a Yukawa well is not compatible, and the exponential well is a borderline case.

For completeness, we have also listed in Table V the well depth parameter s (defined by Jackson and Blatt[19]) for the n-p and p-p singlet interactions. We see that $s^{(n-p)}$ is a few percent larger than $s^{(p-p)}$ for all three potential well shapes. This result reiterates with slightly more force the same result already obtained by Bethe[1] from a comparison of $a_s^{(n-p)}$ and $a_s^{(p-p)}$ assuming equal singlet n-p and p-p intrinsic ranges.

TABLE V. The singlet effective range r_{0s}, intrinsic range b_s, and well depth parameter s, for the n-p singlet interaction (obtained from this experiment) and for the p-p singlet interaction (Jackson and Blatt).

Well shape	$r_{0s}^{(n-p)}$ (10^{-13} cm)	$r_{0s}^{(p-p)}$ (10^{-13} cm)	$b_s^{(n-p)}$ (10^{-13} cm)	$b_s^{(p-p)}$ (10^{-13} cm)	$s^{(n-p)}$	$s^{(p-p)}$
Square	2.47±0.20	2.60±0.07	2.37±0.19	2.58±0.06	0.926±0.006	0.889±0.003
Exponential	2.30±0.21	2.67±0.07	2.17±0.20	2.51±0.06	0.937±0.006	0.907±0.003
Yukawa	2.03±0.23	2.76±0.07	1.90±0.21	2.47±0.06	0.953±0.006	0.922±0.003

[18] For the purposes of this interpretation, the probable error of σ has been increased by an amount that reflects the present experimental uncertainties in a_s, a_t and r_{0t}.

[19] J. D. Jackson and J. M. Blatt, Revs. Modern Phys. **22**, 77 (1950).

[20] See reference 2. Blatt and Jackson also give formulas with which $b_s^{(n-p)}$ can be computed from the values of r_{0s} and a_s for each of the assumed well shapes.

Schwinger[21] has given a possible explanation of this small difference in potential well depth in terms of the different electromagnetic interactions that are present in the n-p and p-p systems.

It is profitable at this point to dwell upon the dependence of the cross section on shape. The shape dependence is manifested through the triplet and singlet parameters P_t and P_s (the shape dependent terms in the expansion of $k\cot\delta$ of order k^6 or higher can be neglected at $E_n=4.75$ Mev). These parameters as obtained from the formulas of Blatt and Jackson[2] are as follows:

Well shape:	S	S.I.	E	Y
P_t:	-0.040	0	$+0.029$	$+0.137$
P_s:	-0.03	0	$+0.010$	$+0.055$

Most of the shape dependence of σ comes from the parameter P_t rather than P_s since $\sigma_t\simeq 3\sigma_s$. Note that a positive value of P decreases the triplet cross section but increases the singlet cross section as compared to $P=0$, since the triplet and singlet scattering amplitudes have opposite signs. Hence, it follows that a pure Yukawa well shape for the triplet potential coupled with any of the shapes other than Yukawa for the singlet potential will imply a value for $r_{0s}{}^{(n-p)}$ even smaller than the one given in Table I, which assumed Yukawa shapes for both singlet and triplet interactions. Stated in another way, this experiment indicates that the Yukawa well value of $P_t=0.137$ coupled with any reasonable value of P_s implies that $r_{0s}{}^{(n-p)}<r_{0s}{}^{(p-p)}$; hence, that charge independence is not valid.

Since the hypothesis of charge independence has the great virtue of simplicity and is at least qualitatively valid, and since the Yukawa form for the nuclear potential is the most satisfying from the meson theoretic point of view, it seems pertinent at this point to ask whether both ideas can be maintained without contradicting the results of this experiment. One simplification of the theoretical analysis of this experiment is the omission of tensor forces in the triplet interaction. The influence of tensor forces on the shape dependent factor P_t has recently been investigated[22] for a particular choice of central and tensor Yukawa potentials. The potential parameters were chosen from the tables of Feshbach and Schwinger[23] so that all low energy parameters including the deuteron quadrupole moment were given correctly, and so that the ratio of tensor range to central range was a maximum. The shape dependent coefficient was found to be 0.14 ± 0.04 as compared with 0.137 for a pure central Yukawa well. Hence, the triplet shape-dependent parameter P_t does not appear to be sensitive to the presence of tensor forces.†

Next we have considered the effect of a repulsive core on the value of the parameter P_t. The idea of a repulsive core was introduced by Jastrow[24] in an attempt to preserve the hypothesis of charge independence while comparing high energy n-p and p-p scattering, and therefore it seemed plausible to inquire whether the repulsive core could accomplish the same purpose of 4.75 Mev. For ease of computation a Hulthén potential displaced from the origin by a repulsive core of variable width b_c was used. The results for a displaced Yukawa well will certainly be similar. The potential had the form

$$V(r)=\begin{cases}+\infty, & r<b_c;\\ -W\dfrac{e^{-\xi(r-b_c)}}{1-e^{-\xi(r-b_c)}}, & r>b_c.\end{cases}\tag{20}$$

For each value of b_c the parameters W and ξ were chosen so as to fit the experimental values of the deuteron binding energy and the effective range $\rho_t(0,-\epsilon)$; $\rho_t(-\epsilon,-\epsilon)$ was evaluated from its definition[3] in terms of the simple bound state wave function for this potential. Next one can define P_t by the equation

$$\rho_t(-\epsilon,-\epsilon)=\rho_t(0,-\epsilon)+2P_t r_{0t}{}^3\gamma^2,\tag{21}$$

where terms of higher order in $(\gamma r_{0t})^2$ have been dropped. One then obtains P_t as a function of the size of the repulsive core b_c. This is shown in Fig. 15. At $b_c=0$, i.e., no repulsive core, $P_t=+0.11$ as compared with $+0.137$ for a pure Yukawa well. P_t falls steeply to 0 at $b_c=0.28\times10^{-13}$ cm, and then approaches its limiting[25] value of -0.049 at the maximum repulsive core ($b_c=1.06\times10^{-13}$ cm) consistent with the low energy scattering parameters. As the size of the repulsive core increases, the depth of the Hulthén potential increases, and the parameter $1/\xi$ decreases, so as to maintain the values of ϵ and $\rho_t(0,-\epsilon)$. This calculation shows that a small repulsive core, $b_c\simeq0.3\times10^{-13}$ cm, which decreases the parameter $1/\xi$ by two thirds, can reduce a large positive value of P_t to zero. Such a reduction in P_t and correspondingly in P_s would yield a value for $r_{0s}{}^{(n-p)}=2.4\pm0.22$, which is smaller than, but certainly not inconsistent with, the corresponding value of

[21] J. Schwinger, Phys. Rev. **78**, 135 (1950).
[22] W. C. Guindon and G. Snow (private communication).
[23] H. Feshbach and J. Schwinger, Phys. Rev. **84**, 194 (1951).
† *Note added in proof:*—J. Blatt has kindly informed us that L. Biedenharn has calculated the shape coefficients for three other choices of tensor and central Yukawa potentials. The value obtained for P_t varied from 0.053 to 0.096. More extensive calculations are clearly necessary in order to determine the importance of tensor forces with respect to the shape dependent coefficients.
[24] R. Jastow, Phys. Rev. **81**, 165 (1951).
[25] These limiting values for b_c and P_t are valid for any well shape displaced from the origin by an infinite repulsive core. Such a limit corresponds to assigning the value of the logarithmic derivative of the wave function at a finite distance as discussed by Breit and Bouricius [Phys. Rev. **75**, 1029 (1949)] for the singlet interaction. The maximum value of b_c can be derived from the general formulas that relate (a, r_0), the scattering amplitude and effective range for a given potential displaced by a repulsive core, to (a', r_0') the same quantities for the given potential without repulsive core. One can show that

$$a=a'+b_c;\quad r_0=r_0'\left(\frac{a'}{a}\right)^2 2b_c+\left(\frac{1-b_c+b_c^2}{a\quad 3a^2}\right).$$

$r_{0s}^{(p-p)}$. Since the limiting value of P_t is negative and only slightly larger in magnitude than the square well value for P_t, all values of b_c larger than 0.3×10^{-13} cm will also be consistent with the hypothesis of charge independence. Hence, we see that the Yukawa-type shape and charge independence can both be maintained if we assume a repulsive core. This should not be construed as definite evidence for a repulsive core, since either the hypothesis of charge independence or the assumption of a Yukawa tail may be wrong.

A recent measurement of the total n-p cross section at 14 Mev by Poss *et al.*[26] led[17] to a mean effective range $r_{0s}^{(n-p)}=2.2\pm0.35\times10^{-13}$ cm. At this energy, the values of $r_{0s}^{(n-p)}$ for the three well shapes (S), (E), and (Y) differ from each other by much less than the probable error. Another pertinent experiment in progress is a measurement[27] of the total n-p cross section at 1.32 Mev. They obtain the tentative result $r_{0s}^{(n-p)}=2.2\pm0.3\times10^{-13}$ cm in the shape independent approximation. These measurements, as well as the present measurement, are consistent with the less accurate results[3] obtained from the experiment of Lampi *et al.*[4]

Measurements by Poss and Storrs seem to imply a failure of the hypothesis of charge independence of nuclear forces. A repetition of the 14-Mev experiment and the completion of the 1.3-Mev experiment may well serve as definitive tests of this hypothesis. Unfortunately, the more or less shape-insensitive value for $r_{0s}^{(n-p)}$ obtained so far from these two experiments falls just in the middle of the range of values obtained for $r_{0s}^{(n-p)}$ from the present experiment. Hence, as the matter now stands, all three potential well shapes, (S), (E), and (Y), as well as all shapes that give equivalent P values, are consistent with all the medium energy n-p data. Finally, it is possible that the value of $r_{0s}^{(n-p)}$ will eventually be measured in a way that is more independent of shape parameters. If so it will, when combined with the measurement reported here, yield an approximate value of the parameter characteristic of the shape of the triplet n-p potential.

We are indebted to Professor D. H. Frisch for his collaboration in the early stages of the experiment, and thereafter for many invaluable suggestions and criticisms. The assistance of Dr. H. L. Poss in the initial phases was also considerable. We are grateful to Dr. E. O. Salant for originally suggesting this experiment, to Dr. H. S. Snyder for discussions about calculations with a repulsive core, to Dr. C. P. Baker for discussion of the entire problem, to Dr. R. Davis, Jr., for the evaporation of CaF_2 targets, to Dr. G. J. Dienes for extensive discussion of the properties of polyethylene, to Mr. R. G. Fulton of the Bakelite Company for infrared spectroscopy, to Dr. R. A. Paulson of the Bureau of Standards for chemical analysis, to Miss Jean Snover for numerical calculations, and to Mr. Frank Marder for construction of the thin-walled target.

[26] Poss, Salant, Snow, and Yuan, Phys. Rev. **87**, 11 (1952).
[27] C. L. Storrs and D. H. Frisch, Massachusetts Institute of Technology Progress Report, May 21, 1952 (unpublished).

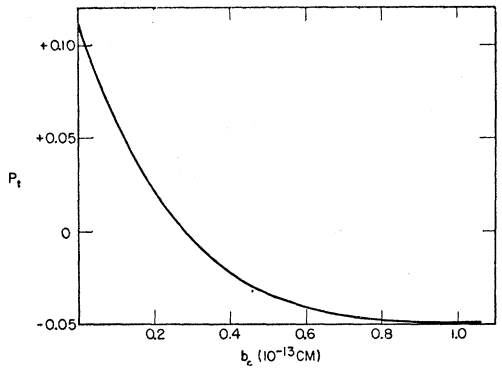

FIG. 15. Shape dependent coefficient P_t for a Hulthén potential displaced from the origin by a repulsive core of width b_c (10^{-13} cm), as a function of b_c. The potential is always adjusted to give correct ϵ and a_t (see text).

APPENDIX I. PILE-UP CALCULATION

Assume that the differential pulse-height spectrum at the discriminator of the detector system can be represented by a distribution of the form

$$f(E)=A(E+\epsilon)^{-\eta}, \tag{22}$$

where E is the pulse height and A, ϵ, and η are arbitrary constants. The integral counting rate *vs* bias is then

$$n(E)=\int_E^\infty f(E)dE=[A/(\eta-1)](E+\epsilon)^{1-\eta}, \tag{23}$$

where, if N is the counting rate at the bias setting E_0, $A=N(\eta-1)(E_0+\epsilon)^{\eta-1}$. Now the rate of pile-up of two pulses smaller than E_0 and of duration τ is

$$P_1=\tau\int_0^{E_0}\int_{E_0-x}^{E_0}A(x+\epsilon)^{-\eta}A(y+\epsilon)^{-\eta}dydx. \tag{24}$$

The integral bias curve observed with our system, Fig. 4, is a good fit to the function (23) if one takes $\epsilon=10.5$ volts and $\eta=2.8$. In order to perform the integrations indicated in (24), we have taken, $\eta=3$ and obtained

$$P_1=\tau N^2\left\{1+2\frac{(k+1)^2}{(k+2)^4}[6\ln(k+1)-(k+2)(4+k-2k^2)]\right\},$$

where $k=E_0/\epsilon$. The rate of pile-up of two pulses larger than E_0 is simply $P_2=\tau N^2$, and the net effect is therefore

$$P=P_1-P_2$$
$$=2\tau N^2\frac{(k+1)^2}{(k+2)^4}[6\ln(k+1)-(k+2)(4+k-2k^2)]. \tag{25}$$

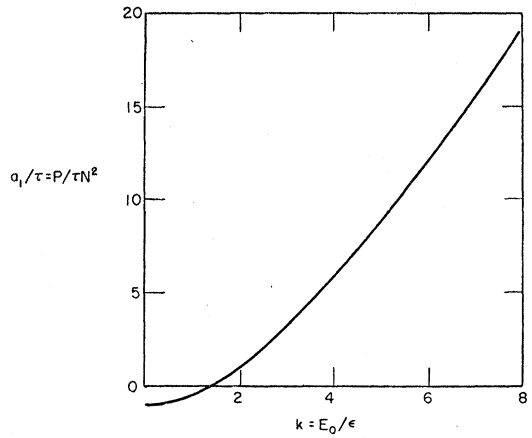

FIG. 16. Rate of pile-up of two pulses, as a function of discriminator bias, for the pulse-height spectrum of neutrons detected in this experiment.

The quantity P/N^2, which can be identified with the coefficient a_1 of Eq. (4), is roughly quadratic in k, rising from the value $-\tau$ at $k=0$ through zero at $k=1.4$ to $+\tau$ at $k=2$ (see Fig. 16). Transmission measurements on channel D1 were made at $E_0=15$ volts, $k=1.4$; pile-up of this type is therefore not expected to enter the experiment.

APPENDIX II. CORRECTION FOR HYDROGEN BACKGROUND

Using the notation of Fig. 2, adopt the following definitions:

A. With deuterium in the target chamber, let

U = unattenuated total count rate,
φU = unattenuated count rate from d-d neutrons produced in the gas,
βU = total count rate with perfect shadow,
$T^0 U$ = total count rate with a scatterer whose true transmission for the component φ is T and whose true transmission for the components $(\gamma_1+\gamma_2)$ is T_{12},
$\gamma_1 U$ = unattenuated count rate for neutrons produced in collimating slits,
$\gamma_2 U$ = unattenuated count rate for neutrons produced in gold end-wall of target.

B. With hydrogen in the target chamber, assume that γ_1 and γ_2 are the same in intensity and in energy as they were in A. Then, with reference to the same scatterer, let

pU = unattenuated total count rate,
$\gamma_3 U$ = unattenuated count rate from d-d neutrons produced in traces of D_2 arising from exchange of H_2 in target walls,
δU = total count rate with perfect shadow,
$pT_p^0 U$ = total count rate with scatterer in.

According to the definitions,

$$\gamma_1+\gamma_2+\varphi+\beta=1, \quad \text{and} \quad \gamma_1+\gamma_2+\gamma_3+\delta=p. \tag{26}$$

Now $T^0=\varphi T+(\gamma_1+\gamma_2)T_{12}+\beta$, implying, together with (26), that

$$T=T^0+(\gamma_1+\gamma_2)(T-T_{12})-(1-T)\beta. \tag{27}$$

The hydrogen background correction is contained in the second term and can be made from direct measurement of γ_1, γ_2, and T_{12}, using a first approximation for T. However, it is important to note that the correction can be made in the presence of an arbitrary amount of γ_3. Observe that

$$pT_p^0=(\gamma_1+\gamma_2)T_{12}+\gamma_3 T+\delta. \tag{28}$$

Using (26) and (28), consider

$$p(T-T_p^0)=(\gamma_1+\gamma_2)(T-T_{12})-(1-T)\delta. \tag{29}$$

Subtracting (29) and (27), one obtains

$$T=T^0+p(T-T_p^0)-(1-T)(\beta-\delta). \tag{30}$$

Thus, the correction can be made from the total hydrogen count p and the corresponding transmission T_p^0. It has been assumed here that the neutrons involved in γ_3 have the same mean energy as those in φ. This is true to the extent that the deuterium fraction entering the hydrogen filling is uniformly distributed through the target volume.